Meccanica (2005) 40: 233–249
DOI 10.1007/s11012-005-4664-7

Active Optics: Vase or Meniscus Multimode Mirrors and Degenerated Monomode Configurations

GÉRARD R. LEMAÎTRE*
Observatoire Astronomique Marseille Provence, Université de Provence Aix Marseille I, 2 Place Le Verrier, F-13248 Marseille CX4, France

(Received: 23 March 2004; accepted in revised form: 17 January 2005)

Abstract. Multimode deformable mirrors allow to superpose optics aberration modes up to high orders. The elasticity analysis leads to consider mainly Clebsch–Zernike modes that belong to a sub-class of optics modes. Theoretical results and associated geometries are also derived for some single modes. This allows discovering degenerated configurations using a minimal set of applied external forces. We present interferometric results from active optics experiments including the degenerated configurations for third-order astigmatism and fifth-order triangle modes.

Key words: Active optics, Aspheric mirrors, Multimode deformable mirrors, Optical aberrations, Elasticity.

1. Introduction and Active Optics Methods

Active optics methods applied to the design and construction of optical mirrors are of particular interest because they naturally provide *smooth* and *accurate* optical surfaces. Compared to the conventional method of generating aspherics, active optics allows avoiding the zonal defects of slope discontinuities due to inherent local polishing tools. Then, such optical surfaces are generated free from high spacial frequency errors. The aspherized optical surface can be used: (i) after *stress polishing* when in a relaxed state, (ii) during *in situ stressing* after a spherical polishing, or, (iii) under a combination of the two cases.

Active methods also provides as well axisymmetrical surfaces or non-axisymmetrical surfaces. Current applications and developments of active optics are in the following fields:

1. large amplitude aspherization by *stress polishing* and/or by *in situ deformation* [1–8],
2. *in situ compensation* of deflections due the orientation of optics in the field gravity [9–11],
3. availability of a *variable asphericity* for various focii selected by mirror interchanging [1, 2],
4. field compensation and cophasing by *variable curvature* for optical telescope arrays [2, 4],

* Author for correspondence: e-mail: gerard.lemaitre@oamp.fr

5. segments and gratings obtained by *replication techniques* from active submasters [1–3],
6. mirror *conceptual models* for optical mode corrections with *adaptive optics systems*.

The case of obtaining non-axisymmetric mirrors such as off-axis mirrors defined locally from an axisymmetric shape, or on-axis mirrors for correcting the aberrations of a non-centred system requires the simultaneous correction of several wavefront modes. In the present linear domain, this is achieved by elastic mode coaddition.

1.1. Remark on Mirror Substrate Manifolds

Given the difficulty of superposing many optical modes with mirror substrates belonging to the *variable thickness distribution* (VTD) class, we emphasize the fact that mirror substrates belonging to the *constant thickness distribution* (CTD) class do provide accurately this superposition capability. Thus, we only consider hereafter mirrors belonging to the CTD class.

2. Concept of Multimode Deformable Mirrors

We consider a plate or a slightly curved meniscus of clear aperture radius a and constant thickness t_1; this defines the active surface of a Multimode Deformable Mirror (MDM). The practicable external loads are the three following cases:

- contour axial forces V_a and contour bending moments M_a without uniform loading, i.e. $q = 0$,
- uniform loading $q = constant$ applied onto all the clear aperture, in reaction at the edge $r = a$,
- the coaddition of the two previous loadings.

The alternatives for MDM geometries are (i) a *meniscus form* plane or moderately curved and (ii) a *vase form* plane or moderately curved:

- A meniscus form is designed with a single plate or a meniscus of semi clear aperture $r = a$. Radial arms in number k_m are clamped to its edge at $r = a$ in order to generate the multimode deformations by applying $F_{a,k}$ and $F_{c,k}$ external forces on each arm k at its ends $r = a$ and c. This design has been developed [5, 6] for the stress-polishing of the mirror segments of the Keck Telescope where 36 of them constitute a 10 m aperture paraboloid primary mirror; each segment is a superposition of the two aberration modes $Astm\,3$ and $Coma\,3$.
- A vase form MDM is designed with an inner meniscus providing the optics clear aperture of diameter $2a$, and an outer ring clamped to the edge of the inner meniscus. Radial arms in number k_m are clamped to ring outer radius $r = b$. Discrete forces $F_{a,k}$ are applied at $r = a$ onto the rear side of the ring; a same number of $F_{c,k}$ forces are applied onto the end of the arm at $r = c$. The azimuth location θ of the arms is defined by the integer k belonging to the numbers $1, 2, 3, \ldots, k_m$ for a k_m-arm MDM, with $\theta = 0 \Leftrightarrow k = 1$ (Figure 1).

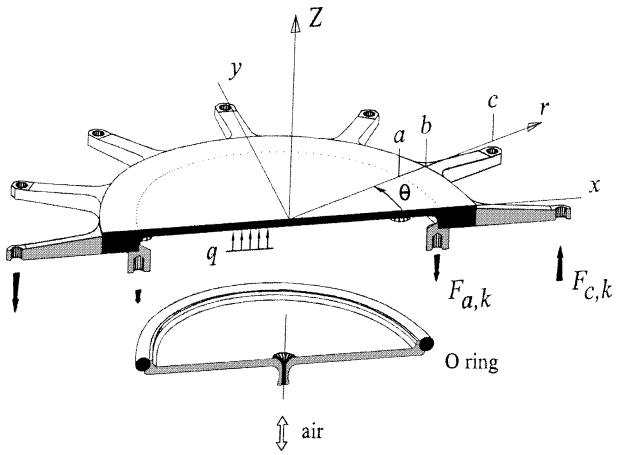

Figure 1. Elasticity design of a *vase form* MDM. Clear aperture $2a$. Concentric zones of thicknesses t_1 at $0<r<a$, and t_2 at $a<r<b$. Radial arms $k_m=12$. With respect to Saint–Venant's principle, the forces are applied as far as possible from the optical surface in order to prevent from local deformations due to the shear component of the flexure.

3. MDM Elasticity Theory and Clebsch–Zernike Modes

The MDMs use constant thickness plates and rings, thus, for moderate curvatures and thicknesses, the equation of deflection for small deformations Z is

$$\nabla^2\nabla^2 Z(r,\theta)=q/D \quad \text{with} \quad D=Et^3/[12(1-\nu^2)]=constant, \tag{1}$$

where ∇^2 is the laplacian, q the uniform loading, and D the rigidity.

With vase forms, two rigidities are necessarily considered $D=D_1$ for $0<r<a$ (inner zone) and $D=D_2$ for $a<r<b$ (outer zone), with corresponding thicknesses t_1 and t_2 respectively. E, is the Young's modulus and ν is the Poisson's ratio.

3.1. Inner Zone

For simplification, we avoid here the $\sin m\theta$ function terms that provide similar solutions rotated of $\theta=\pi/2$ in the cylindrical coordinate system and would allow generating deformation modes in any given azimuth. Thus, we consider flexure modes that are identical to optical modes and defined by

$$Z=\sum z_{nm}=\sum A_{nm}r^n\cos m\theta, \quad n+m \text{ even}, \quad m\leqslant n, \tag{2}$$

where n and m are positive integers. Since the optical modes – dioptric modes and aberration modes – representing a wavefront are represented from a triangle matrix defined by $n+m$ even and $m\leqslant n$, we will consider hereafter an identical triangle matrix for A_{nm} coefficients of the flexure modes, i.e. with the same composition rules for n and m.

Given a mode z_{nm}, by substitution in the 4th derivative equation, we obtain:

$$A_{nm}(n^2-m^2)[(n-2)^2-m^2]r^{n-4}\cos m\theta=q/D \tag{3}$$

with $n \geqslant 2$. The only combinations of n and m for which the equation can be solved are:

- case $q = 0 \rightarrow m = n$ i.e. $A_{22}, A_{33}, A_{44}, \ldots$ terms,
  $\rightarrow m = n - 2$ i.e. $A_{20}, A_{31}, A_{42}, \ldots$ terms,
- case $q = constant \rightarrow n = 4, \quad m = 0$ i.e. the A_{40} term.

These two cases define a *sub-class* proposed to be called Clebsch–Zernike modes. Except for the z_{40} mode, these modes are the two lower diagonals of the optics triangle matrix.

3.2. Outer Zone

The flexure of the outer ring, which is in a clamped link with the inner zone, is represented by

$$Z = \sum z_{nm} = R_{n0} + \sum_{m=1}^{\infty} R_{nm} \cos m\theta, \tag{4}$$

where $R_{nm}(r)$ satisfy the Clebsch's equation [12]

$$\left(\frac{d^2}{dr^2} + \frac{1}{r}\frac{d}{dr} - \frac{m^2}{r^2}\right)\left(\frac{d^2 R_{nm}}{dr^2} + \frac{1}{r}\frac{dR_{nm}}{dr} - \frac{m^2}{r^2} R_{nm}\right) = 0, \tag{5}$$

and have the following forms:

$$R_{n0} = B_{n0} + C_{n0} \ln r + D_{n0} r^2 + E_{n0} r^2 \ln r, \tag{6a}$$

$$R_{n1} = B_{n1} r + C_{n1} r^{-1} + D_{n1} r^3 + E_{n1} r \ln r, \tag{6b}$$

$$R_{nm} = B_{nm} r^m + C_{nm} r^{-m} + D_{nm} r^{m+2} + E_{nm} r^{-m+2}, \tag{6c}$$

3.3. Boundary Conditions

The boundaries between the two zones at $r = a$ must provide a continuity of the flexure z_{nm}, slope dz_{nm}/dr, bending moment M_r and net shearing force V_r. The radial and tangential bending moments M_r, M_t, and the twisting moment M_{rt} are, respectively, defined by

$$M_r = D\left[\frac{\partial^2 z}{\partial r^2} + \nu\left(\frac{1}{r}\frac{\partial z}{\partial r} + \frac{1}{r^2}\frac{\partial^2 z}{\partial \theta^2}\right)\right], \tag{7a}$$

$$M_t = D\left[\frac{1}{r}\frac{\partial z}{\partial r} + \frac{1}{r^2}\frac{\partial^2 z}{\partial \theta^2} + \nu\frac{\partial^2 z}{\partial r^2}\right], \tag{7b}$$

$$M_{rt} = (1 - \nu) D\left[\frac{1}{r^2}\frac{\partial z}{\partial \theta} - \frac{1}{r}\frac{\partial^2 z}{\partial r \partial \theta}\right]. \tag{7c}$$

This representation of the flexural moments entails a positive flexure if a positive radial bending moment is M_r is applied at $r = a$ for generating the fundamental mode z_{20} (curvature mode). For z_{nm} modes with $m = n$, we may also verify that M_r is positive in the x, z section i.e. if $y = \theta = 0$. This sign convention is natural and also in agreement with

the generally used optics convention of a positive curvature if an optical surface belongs to the positive space of z axis when its vertex is at the origin $z=0$.

The radial and tangential shearing forces Q_r and Q_t are derived from the static equilibrium of the moments at the elementary segment $\mathrm{d}r\, r\, \mathrm{d}\theta$ around the radial and tangential axes passing by the origin. These are, respectively,

$$Q_r = -\frac{\partial M_r}{\partial r} - \frac{1}{r}\left(M_r - M_t - \frac{\partial M_{rt}}{\partial \theta}\right) = -D\frac{\partial}{\partial r}(\nabla^2 z), \tag{8a}$$

$$Q_t = -\frac{1}{r}\left(\frac{\partial M_t}{\partial \theta} - 2M_{rt}\right) + \frac{\partial M_{rt}}{\partial r} = -D\frac{1}{r}\frac{\partial}{\partial \theta}(\nabla^2 z), \tag{8b}$$

where the second equalities on left-hand side are obtained by substitutions of the moments using their representation in equations (7a)–(7c).

The equilibrium of the shearing forces with the external and uniform load q demonstrates the Poisson biharmonic equation

$$q = -\frac{1}{r}\left[\frac{\partial}{\partial r}(r\,Q_r) + \frac{\partial Q_t}{\partial \theta}\right] = D\nabla^2\nabla^2 z. \tag{8c}$$

The net shearing force V_r, derived by the Kirchhoff condition when a twisting moment M_{rt} exists into the plate, is represented by [1]

$$V_r = Q_r - \frac{1}{r}\frac{\partial M_{rt}}{\partial \theta}. \tag{9a}$$

This force allows the correct determination of the acting or reacting force existing at the boundaries. After substitution of Q_r and M_{rt}, we obtain

$$V_r = -D\frac{\partial}{\partial r}(\nabla^2 z) + (1-\nu)D\frac{1}{r}\frac{\partial}{\partial r}\left(\frac{1}{r}\frac{\partial^2 z}{\partial \theta^2}\right). \tag{9b}$$

Let us denote γ the rigidity-ratio between the two zones as

$$\gamma = \frac{D_1}{D_2} = \frac{t_1^3}{t_2^3}, \quad \gamma < 1 \text{ for a vase form.} \tag{9c}$$

The previous relations allow writing the continuity conditions of the two zones at $r=a$. The continuity of ordinates, slopes, bending moments and net shearing forces are, respectively, represented by

---

[1] The present definition of the net shearing force V_r allows predicting the degenerated configurations presented hereafter in Sections 4 and 6 where these results are experimentally verified.
There is an error in *Theory of Plates and Shells* by Timoshenko and Woinowsky–Krieger at Equation (j) p. 284: Their convention uses an opposite sign in the definition of the three moments M_r, M_t, and M_{rt} while the sign of their shearing forces Q_r and Q_t with respect to the Laplacian term is as above equations (8a) and (8b), so that the two equations in (8c) are the same. Hence the correctly associated representation of the net shearing force should be $V_r = Q_r + \partial M_{rt}/(r\partial r)$, with their notation.

$$A_{nm}a^n = R_{nm}(a), \tag{10a}$$

$$A_{nm}na^{n-1} = \left[\frac{dR_{nm}}{dr}\right]_{r=a}, \tag{10b}$$

$$A_{nm}[n(n-1)+\nu(n-m^2)]a^{n-2} = \frac{1}{\gamma}\left[\frac{d^2R_{nm}}{dr^2}+\frac{\nu}{r}\frac{dR_{nm}}{dr}-\frac{\nu m^2}{r^2}R_{nm}\right]_{r=a}, \tag{10c}$$

$$A_{nm}[(n-2)(n^2-m^2)+(1-\nu)(n-1)m^2]a^{n-3} = -\frac{1}{\gamma}[V_r(R_{nm})]_{r=a}. \tag{10d}$$

This equation set allows to solve B_{nm}, C_{nm}, D_{nm} and E_{nm} as functions of A_{nm} in order to determine the distributions of bending moments $M_r(b,\theta)$ and net shearing forces $V_r(b,\theta)$ to apply at the ring edge $r=b$.

For the first Clebsch–Zernike modes, these determinations lead to the following relationships:

Curvature 1st-order mode - *Cv*1, $n=2, m=0$,

$$\begin{aligned}
B_{20} &= (1-\gamma)(1+\nu)(1-\ln a^2)a^2A_{20}/2,\\
C_{20} &= (1-\gamma)(1+\nu)a^2A_{20},\\
D_{20} &= [2-(1-\gamma)(1+\nu)]A_{20}/2,\\
E_{20} &= 0,\\
M_r(b,0) &= D_2[-(1-\nu)C_{20}/b^2+2(1+\nu)D_{20}+(3+\nu)E_{20}+(1+\nu)E_{20}\ln b^2],\\
Q_r(b,0) &= -4D_2E_{20}/b,\\
V_r(b,0) &= Q_r(b,0).
\end{aligned} \tag{11a}$$

Spherical aberration 3rd-order mode - *Sphe* 3, $n=4, m=0$, with $q=64D_1A_{40}$,

$$\begin{aligned}
B_{40} &= \{\nu+\gamma(5-\nu)-[(1+\nu)+\gamma(1-\nu)]\ln a^2\}a^4A_{40},\\
C_{40} &= 2[(1+\nu)+\gamma(1-\nu)]a^4A_{40},\\
D_{40} &= [1-\nu-\gamma(5-\nu+4\ln a^2)]a^2A_{40},\\
E_{40} &= 8\gamma a^2A_{40},\\
M_r(b,0) &= D_2[-(1-\nu)C_{40}/b^2+2(1+\nu)D_{40}+(3+\nu)E_{40}+(1+\nu)E_{40}\ln b^2],\\
Q_r(b,0) &= -4D_2E_{40}/b,\\
V_r(b,0) &= Q_r(b,0).
\end{aligned} \tag{11b}$$

Coma 3rd-order mode – *Coma* 3, $n=3, m=1$,

$$\begin{aligned}
B_{31} &= (1-\gamma)[3+\nu-(1-\nu)\ln a^2]a^2A_{31}/2,\\
C_{31} &= -(1-\gamma)(1+\nu)a^4A_{31}/2,\\
D_{31} &= \gamma A_{31},\\
E_{31} &= (1-\gamma)(1-\nu)a^2A_{31},\\
M_r(b,0) &= D_2[2(1-\nu)C_{31}/b^3+2(3+\nu)D_{31}b+(1+\nu)E_{31}/b],\\
Q_r(b,0) &= -2D_2[4D_{31}-E_{31}/b^2],\\
V_r(b,0) &= -D_2[-2(1-\nu)C_{31}/b^4+2(5-\nu)D_{31}-(1+\nu)E_{31}/b^2].
\end{aligned} \tag{11c}$$

Astigmatism 3rd-order mode – *Astm* 3, $n=2, m=2$,

$$\begin{aligned}
B_{22} &= [4+(1-\gamma)(1-\nu)]A_{22}/4,\\
C_{22} &= -(1-\gamma)(1-\nu)a^4A_{22}/12,\\
D_{22} &= -(1-\gamma)(1-\nu)a^{-2}A_{22}/6,\\
E_{22} &= 0,\\
M_r(b,0) &= 2D_2[(1-\nu)B_{22}+3(1-\nu)C_{22}/b^4+6D_{22}b^2-2\nu E_{22}/b^2],\\
Q_r(b,0) &= -8D_2[3D_{22}b+E_{22}/b^3],\\
V_r(b,0) &= -4D_2[(1-\nu)B_{22}/b-3(1-\nu)C_{22}/b^5+3(3-\nu)D_{22}b+(1+\nu)E_{22}/b^3].
\end{aligned} \tag{11d}$$

Astigmatism 5th-order mode – *Astm* 5, $n=4, m=2$,

$$\begin{aligned}
B_{42} &= 3(1-\gamma)(3-\nu)a^2A_{42}/4,\\
C_{42} &= -(1-\gamma)(1+\nu)a^6A_{42}/4,\\
D_{42} &= [\gamma-(1-\gamma)(1-\nu)]A_{42}/4,\\
E_{42} &= -3(1-\gamma)(1-\nu)a^4A_{42}/4,\\
M_r(b,0) &= 2D_2[(1-\nu)B_{42}+3(1-\nu)C_{42}/b^4+6D_{42}b^2-2\nu E_{42}/b^2],\\
Q_r(b,0) &= -8D_2[3D_{42}b+E_{42}/b^3],\\
V_r(b,0) &= -4D_2[(1-\nu)B_{42}/b-3(1-\nu)C_{42}/b^5+3(3-\nu)D_{42}b+(1+\nu)E_{42}/b^3].
\end{aligned} \tag{11e}$$

Triangle 5th-order mode – *Tri* 5, $n=3, m=3$,

$$\begin{aligned}
B_{33} &= [2+(1-\gamma)(1-\nu)y]A_{33}/2,\\
C_{33} &= -(1-\gamma)(1-\nu)a^6A_{33}/8,\\
D_{33} &= -3(1-\gamma)(1-\nu)a^{-2}A_{33}/8,\\
E_{33} &= 0,\\
M_r(b,0) &= 2D_2[3(1-\nu)B_{33}b+6(1-\nu)C_{33}/b^5+2(5-\nu)D_{33}b^3+(1-5\nu)E_{33}/b^3],\\
Q_r(b,0) &= -24D_2[2D_{33}b^2+E_{33}/b^4],\\
V_r(b,0) &= -6D_2[3(1-\nu)B_{33}-6(1-\nu)C_{33}/b^6+2(7-3\nu)D_{33}b^2+(1+3\nu)E_{33}/b^4].
\end{aligned} \tag{11f}$$

In order to achieve the bending moments M_r and the net shearing forces V_r at $r=b$, it is to be noticed that the MDM design gains in *compactness* by applying axial forces at $r=a$ and $r=c$ instead of at $r=b$ and $r=c$. With this choice, the axial forces denoted $F_{a,k}$ and $F_{c,k}$ are defined by the statics equilibrium equations

$$F_{a,k}+F_{c,k} = b\int_{\pi(2k-3)/k_m}^{\pi(2k-1)/k_m} V_r(b,\theta)\mathrm{d}\theta, \tag{12a}$$

$$(a-b)F_{a,k}+(c-b)F_{c,k} = b\int_{\pi(2k-3)/k_m}^{\pi(2k-1)/k_m} M_r(b,\theta)\mathrm{d}\theta, \tag{12b}$$

with $k=1,2,\ldots,k_m$ for a MDM having k_m arms. The forces $F_{a,k}$ and $F_{c,k}$ are determined for each mode by solving this system.

The coaddition of various modes is obtained by summing the corresponding forces. The resulting forces to apply $\mathcal{F}_{a,k}$ and $\mathcal{F}_{c,k}$ are

$$\mathcal{F}_{a,k} = \sum_{nm \text{ modes}} F_{a,k} \quad \text{and} \quad \mathcal{F}_{c,k} = \sum_{nm \text{ modes}} F_{c,k}. \tag{13}$$

As an example, Table 1 displays the $F_{a,k}$ and $F_{c,k}$ forces of a 12 arms and 20 cm aperture MDM providing Clebsch–Zernike modes of 0.1 mm PtV sags.

The coaddition mode capability can be used for generating the shape of the secondary and tertiary mirrors of telescopes designed with a liquid primary mirror [13–15] in systems observing off-zenith [16, 17]. This can also be used as recording compensators for the generation of aberration corrected holographic gratings [18–20]. The results of single and some composed Clebsch–Zernike modes obtained with the twelve-arm vase form MDM are displayed by Figure 2 with the optics triangle matrix. The three interferograms on down-left are a coaddition of $z_{20} + z_{40}$, and coadditions of $z_{22} + z_{24}$ modes, respectively.

3.4. Link of Radial Arms to a Vase Form

The axial forces $F_{a,k}$ and $F_{c,k}$ defined by (12a) and (12b), and displayed in the case of Table 1, strictly correspond to a clamped link of the arms into the vase ring along a relatively narrow zone centred at $r = b$; from the design in Figure1, this would require adding an extra axial thickness in order to physically separate the arms from the ring. Since the ring surface is optically useless, it has to be designed relatively narrow for most practi-

Table 1. Vase form and force distribution with a k_m=12-Arm MDM

Angle	Arm	*Cv* 1		*Sph* 3*		*Coma* 3		*Astm* 3		*Astm* 5		*Tri* 5	
	nb.	$n=2$	$m=0$	$n=4$	$m=0$	$n=3$	$m=1$	$n=2$	$m=2$	$n=4$	$m=2$	$n=3$	$m=3$
θ	k	$F_{a,k}$	$F_{c,k}$	$F_{a,k}$	$F_{c,k}$	$F_{a,k}$	$F_{c,k}$	$F_{a,k}$	$F_{c,k}$	$F_{a,k}$	$F_{c,k}$	$F_{a,k}$	$F_{c,k}$
0	1	−113.3	113.3	−464.0	302.4	−84.0	71.6	154.0	−17.0	168.2	29.9	792	37.3
$\pi/6$	2	−113.3	113.3	−464.0	302.4	−72.7	62.0	77.0	−8.5	81.4	14.9	0	0
$\pi/3$	3	−113.3	113.3	−464.0	302.4	−42.0	35.8	−77.0	8.5	−81.4	−14.9	−792	−37.3
$\pi/2$	4	−113.3	113.3	−464.0	302.4	0.0	0.0	−154.0	17.0	−168.2	−29.9	0	0
$2\pi/3$	5	−113.3	113.3	−464.0	302.4	42.0	−35.8	−77.0	8.5	−81.4	−14.9	792	37.3
$5\pi/6$	6	−113.3	113.3	−464.0	302.4	72.7	−62.0	77.0	−8.5	81.4	14.9	0	0
π	7	−113.3	113.3	−464.0	302.4	84.0	−71.6	154.0	−17.0	168.2	29.9	−792	−37.3
$7\pi/6$	8	−113.3	113.3	−464.0	302.4	72.7	−62.0	77.0	−8.5	81.4	14.9	0	0
$4\pi/3$	9	−113.3	113.3	−464.0	302.4	42.0	−35.8	−77.0	8.5	−81.4	−14.9	792	37.3
$3\pi/2$	10	−113.3	113.3	−464.0	302.4	0.0	0.0	−154.0	17.0	−168.2	−29.9	0	0
$5\pi/3$	11	−113.3	113.3	−464.0	302.4	−42.0	35.8	−77.0	8.5	−81.4	−14.9	−792	−37.3
$11\pi/6$	12	−113.3	113.3	−464.0	302.4	−72.7	62.0	77.0	−8.5	81.4	14.9	0	0

* The required uniform loading to generate *Sph*3 mode is $q = 64 D_1 A_{40} = 0.06172$ daN/mm^2.
Ptv Sags: $w = 0.1$mm. FeCr13 stainless steel: $E = 205 \times 10^9$Pa, $\nu = 0.305$. Geometry: $a = 100$ mm, $t_1 = 8$ mm, $b/a = 1.24$, $c/a = 1.8125$, $\gamma = (t_1/t_2)^3 = 1/27$. Coefficients: $A_{20} = w/a^2$, $A_{40} = w/a^4$, $A_{31} = w/2a^3$, $A_{22} = A_{20}/2$, $A_{42} = A_{40}/2$, $A_{33} = A_{31}$.
(Units: daN)

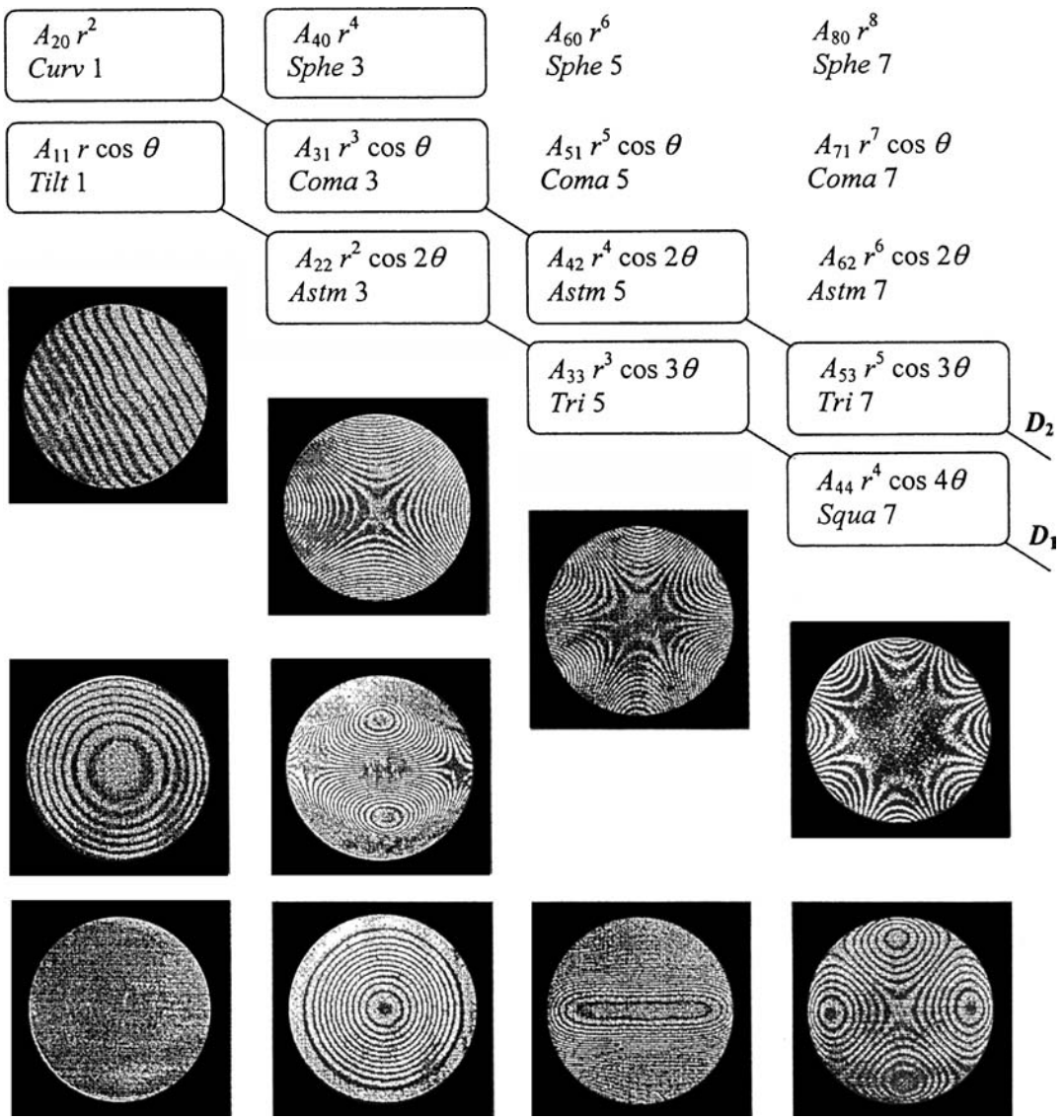

Figure 2. (Up) Diagram showing the distribution of Clebsch–Zernike modes into the optics triangle matrix (1st mode not shown). $\rightarrow q = 0$ provides $m = n$ modes, and $m = n - 2$ modes (D_1 and D_2 diagonals). $\rightarrow q = constant$ provides $m = 0$, $n = 4$ mode (where z_{40} mode is coupled with z_{20} mode). (Down) Deformation interferograms obtained with a 12-arm vase form prototype mirror described in Figure 1 and Table 1. From left to right, the interferograms are as follows: (Up diagonal boxes) *Tilt* 1, *Astm* 3, *Tri* 5 and *Squa* 7 modes, (Middle line boxes) *Curv* 1 and *Coma* 3 modes, (Bottom line boxes) Mirror at rest with respect to a plane, coaddition of *Curv* 1 and *Sphe* 3 modes, coaddition of *Curv* 1, *Sphe* 3 and *Astm* 3 modes, and coaddition of *Astm* 3 and *Squa* 7 modes.

cal applications. Then, using compact designs with integrated arms into the ring thickness from $r = a$ to $r = b$ – such as displayed by Figure 1 – is in quite good agreement with the analysis provided $b/a \leqslant 1.2$ or 1.25. However, for a strict agreement with the force intensities such as derived from the analysis, the inner end of the arms can be partially separated from the ring by making a radial clearance from $r = a$ to a convenient radius $r = a + \kappa(b - a)/(\kappa + 1)$ where $0 < \kappa \leqslant 2$ or 3.

Some particular monomode deformations can be obtained with a vase or a meniscus form by only requiring $F_{c,k}$ forces, i.e. where $F_{a,k}$ forces vanish, thus reducing the number of force points by a factor two. For instance this is the case for z_{22} and z_{33} modes, and more generally for z_{nm} modes provided $m=n$.

Such configurations with a *minimal force-point number* will be found hereafter from the above analysis.

4. Degenerated Configurations for Third-order Astigmatism

In the case of third-order astigmatism $z_{22}=A_{22}r^2\cos 2\theta$, particular configurations can be derived if $F_{a,k}=0$. Since only requiring $F_{c,k}$ forces, this simplify the design by reducing the force number to minimum. Thus, we call them *degenerated configurations*. This condition leads to define the associated ring geometry. For a vase form and a meniscus form, we obtain from Equations (12a) and (12b).

$$(c-b)\int_{\pi(2k-3)/k_m}^{\pi(2k-1)/k_m} V_r(b,\theta)\mathrm{d}\theta=\int_{\pi(2k-3)/k_m}^{\pi(2k-1)/k_m} M_r(b,\theta)\mathrm{d}\theta. \tag{14}$$

After substitution of coefficients for *Astm* 3 mode defined by Equation (11d), the result of calculation shows that such degenerated solutions are provided by the condition

$$\frac{c}{b}=1-\frac{1+(1-\gamma)(1-\nu)\left[\dfrac{1}{4}-\dfrac{1}{1-\nu}\dfrac{b^2}{a^2}-\dfrac{a^4}{4b^4}\right]}{2+(1-\gamma)(1-\nu)\left[\dfrac{1}{2}-\dfrac{3-\nu}{1-\nu}\dfrac{b^2}{a^2}+\dfrac{a^4}{2b^4}\right]} \tag{15}$$

4.1. Meniscus Form

In this case, the rigidity-ratio $\gamma=1$ and we can write $b=a$ since the outer ring vanishes. Therefore, we obtain the following properties

1 → *Two pairs of opposite sets of* $F_{c,k}$ *forces provide Astm 3 if*

$$c/b=c/a=1/2. \tag{16}$$

2 → *With* $k_m=4$ *arms, the intensity and the direction of each force is*

$$F_{c,k}=(-1)^k Et^3A_{22}/3(1+\nu)\quad \textit{with}\quad k=1,2,3,4. \tag{17}$$

The arms are folded to receive the external forces at their ends. The minimum number of arms is $k_m=4$. These solutions can be compared to four-force cycloid-like solutions provided by the Vtd class and using a free-edge warping ring [1–3]. A *meniscus form* mirror with four arms providing an *Astm* 3 mode is displayed by Figure 3.

4.2. Vase Form

The external $F_{c,k}$ forces are applied to the ends $r=c$ of folded arms clamped at $r=b$.

→ *With* $k_m=4$ *arms , the intensity and the direction of each force is*

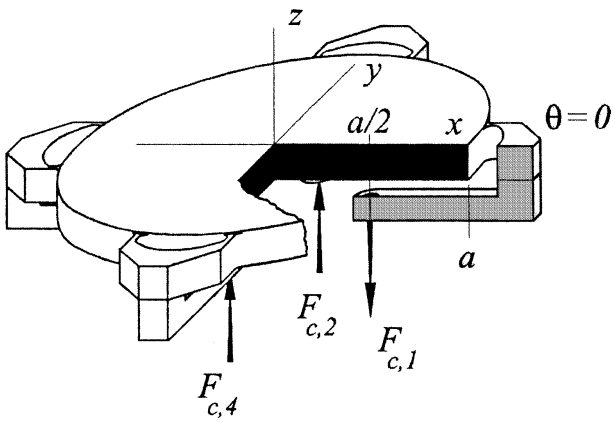

Figure 3. True proportion design of a *meniscus form* mirror with four arms providing an *Astm* 3 deflection. Near the mirror perimeter, the built-in arms have been modified into built-in arches; this achieve a better azimuth modulation in $\cos 2\theta$ for large deformations.

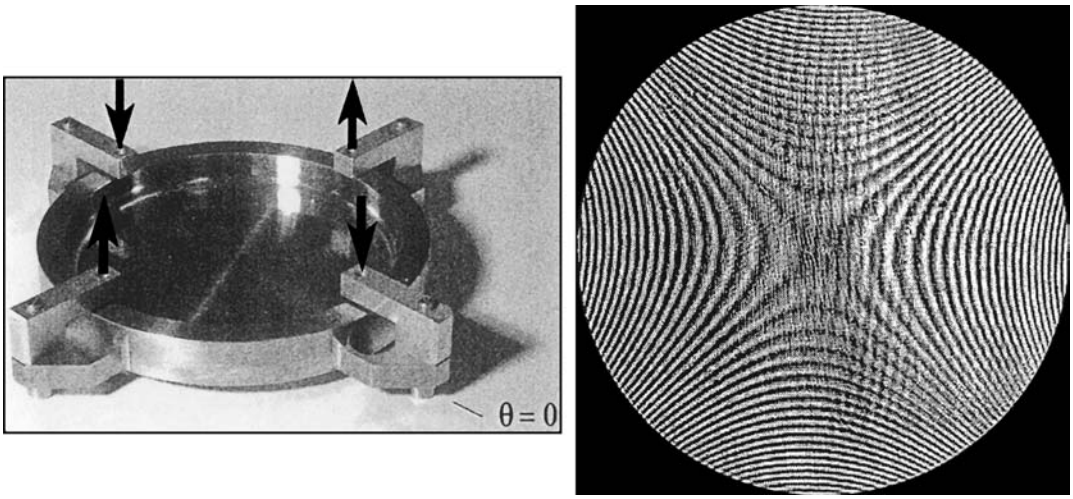

Figure 4. Degenerated configuration of a four-arm *vase form* mirror providing an *Astm* 3 mode deflection. This solution satisfies the condition (15), expressing that $F_{a,k}=0$, then only requires four external forces. Substrate: FeCr13 stainless steel, $\nu=0.305$. Geometry: clear aperture $2a=100\,\text{mm}$, $2a/t_1=20$, $\gamma=1/27$, $b/a=6/5$, $c/b=0.7582$. (*Left*) Rear side view of the mirror. (*Right*) Resulting He–Ne interferogram after deflection. With respect to higher-order modes of the astigmatism family, the reduction of the interferograms shows that the purity of this mode is characterized by $|A_{42}/A_{22}|\leqslant 0.023$ and $|A_{62}/A_{22}|\leqslant 0.005$.

$$F_{c,k}=(-1)^k(1-\gamma)(1-\nu)^2\left[\frac{4}{(1-\gamma)(1-\nu)}+1-2\frac{3-\nu}{1-\nu}\frac{b^2}{a^2}+\frac{a^4}{b^4}\right]D_2A_{22}. \tag{18}$$

With four acting arms as a minimum to achieve this flexure, such a configuration has been designed, built and experienced (Figure 4).

5. Vase Form Mdms for All Reflective Schmidt Telescopes

Wide field All-Reflective Schmidt (ARS) telescopes or cameras does not suffer from the chromatic variation of spherical aberration which is the limitation of conventional Schmidts using a refractive plate as corrector of the associated spherical concave mirror. As for a refractive corrector plate, the reflective plate defines the pupil of incident beams, and its vertex is located at the center of curvature of the concave mirror. Let us consider, with ARSS, a circular correcting mirror as primary mirror.

5.1. CENTERED ARS SYSTEMS

In a centered ARS system, the optical design is of rotational symmetry and the field of view has its center off the telescope axis. Denoting $\rho = r/r_m$ the dimensionless radial variable, the aspherical shape of the primary mirror can be represented by [21]

$$Z_{\mathrm{Opt}} = \frac{r_{\mathrm{m}}}{2^9 \Omega^3 \cos i}(3\rho^2 - \rho^4), \tag{19}$$

where r_{m} is the clear aperture radius and pupil, R is the curvature radius of secondary mirror, $\Omega = f/d = R/4r_{\mathrm{m}}$ is the system f-ratio, and i is the incidence of principal ray at primary.

The A_{nm} coefficients can be defined from

$$Z_{\mathrm{Opt}} = A_{20}\, r^2 + A_{40}\, r^4, \tag{20}$$

so that, from identifications, the $Cv1$ and $Sphe3$ amplitudes are

$$A_{20} = \frac{3}{2^9 \Omega^3 r_{\mathrm{m}} \cos i} \quad \text{and} \quad A_{40} = \frac{-1}{2^9 \Omega^3 r_{\mathrm{m}}^3 \cos i}. \tag{21}$$

The primary mirror can be aspherized by stress polishing as well as by *in-situ* stressing. The coaddition of the two modes is greatly simplified if the radial arms are suppressed, that is

$$F_{c,k}|_{Cv1} + F_{c,k}|_{Sphe3} = 0. \tag{22}$$

For these modes, the analytic expressions of M_r and V_r represented by Equations (11a) and (11b) allow the determination of forces $F_{a,k}$ and $F_{c,k}$ by substitution in (12a) and (12b). Therefore, the condition (22) is satisfied if the *rigidity-ratio* $\gamma = t_1^3/t_2^3$ is defined by

$$\frac{1}{\gamma} = \frac{16\left[2\dfrac{a}{b} - 1 - (1+\nu)\ln\dfrac{a}{b}\right] - (5+\nu)\left[1+\nu+(1-\nu)\dfrac{a^2}{b^2}\right]}{(1-\nu^2)\left(1-\dfrac{a^2}{b^2}\right)}. \tag{23}$$

The resulting geometry of a vase form primary mirror without arms is displayed by Figure 5-Up where an enclosure plate simply supported at its edge allows applying a partial vacuum to the mirror. Design parameters satisfying this equation for a numerical application are displayed by Table 2.

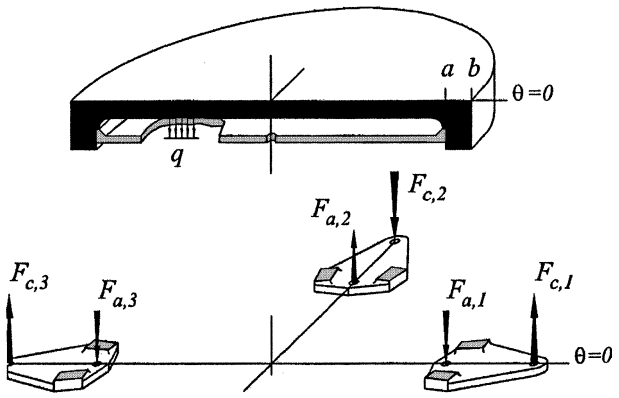

Figure 5. True proportion scheme of a *vase form* as Schmidt primary mirror in Zerodur.(*Up*) The coaddition of *Cv* 1 and *Sphe* 3 modes for a centered system used off-axis does not require radial arms but is just achieved by closing the rear side of sc Mdm if the rigidity-ratio condition is satisfied. (*Down*) The coaddition of *Astm* 3 and *Astm* 5 modes for a non-centered system requires a minimum of four bounded arms in Invar.

Table 2. Examples of parameters for a Schmidt primary mirror with four arms

Angle	Arm	*Cv1*		*Sphe* 3*		*Astm* 3		*Astm* 5	
	nb.	$n=2$	$m=0$	$n=4$	$m=0$	$n=2$	$m=2$	$n=4$	$m=2$
θ	k	$F_{a,k}$	$F_{c,k}$	$F_{a,k}$	$F_{c,k}$	$F_{a,k}$	$F_{c,k}$	$F_{a,k}$	$F_{c,k}$
0	1	−39.318	39.318	64.376	−39.318	−0.231	0.033	0.144	0.040
$\pi/2$	2	−39.318	39.318	64.376	−39.318	0.231	−0.033	−0.144	−0.040
π	3	−39.318	39.318	64.376	−39.318	−0.231	0.033	0.144	0.040
$3\pi/4$	4	−39.318	39.318	64.376	−39.318	0.231	−0.033	−0.144	−0.040

(*) The uniform loading is $q=64D_1A_{40}=-0.000798\,\text{daN mm}^{-2}$.
$F_{c,k}$ are opposite for *Cv* 1 and *Sphe* 3 avoiding radial arms for centered systems ARS.
f-ratio: $\Omega=5$, Clear aperture: $2r_m=2a=400\,\text{mm}$,
Field of view: $2\varphi_m=5^\circ$, Incidence angle: $i=\varphi_m+1/4\Omega=5.35^\circ$.
Elasticity constants of Zerodur: $E=90.6\times10^9\,\text{Pa}$, $\nu=0.240$.
vase-MDM geometry: $t_1=20\,\text{mm}$, $t_2/t_1=(1/\gamma)^{1/3}=2.791$, $b/a=1.150$, $c/a=1.5$.
$A_{20}=2.344\times10^{-5}$, $A_{40}=-1.945\times10^{-10}$, $A_{22}=-1.029\times10^{-7}$, $A_{42}=1.715\times10^{-12}$ in mm^{1-n}.
[Units: daN]

5.2. Non-Centered Ars Systems

We consider a non-centered ARS system with a bi-symmetric primary mirror, a concave spherical secondary and a field of view centered on the central mechanical axis of the secondary. The shape of the primary mirror is represented by [22]

$$Z_{\text{Opt}}=\frac{r_m}{2^9\Omega^3\cos i}[3(1-t)\rho^2-3t\rho^2\cos2\theta-(1-2t)\rho^4+2t\rho^4\cos2\theta], \tag{24}$$

where $i=\varphi_m+1/4\Omega$ for an unfolded ARS. The deviation angle $2i$ of the principal ray should be larger if a flat folding holed-mirror is used to give outside access to the focus.

If defining the primary mirror figure from

$$Z_{\mathrm{Opt}} = \sum A_{nm} r^n \cos m\theta, \tag{25}$$

then, the first A_{nm} mirror coefficients are

$$\begin{aligned} A_{20} &= \frac{3(1-t)}{2^9 \Omega^3 r_{\mathrm{m}} \cos i}, \quad A_{40} = \frac{-(1-2t)}{2^9 \Omega^3 r_{\mathrm{m}}^3 \cos i}, \\ A_{22} &= \frac{-3t}{2^9 \Omega^3 r_{\mathrm{m}} \cos i}, \quad A_{42} = \frac{2t}{2^9 \Omega^3 r_{\mathrm{m}}^3 \cos i}. \end{aligned} \tag{26}$$

Four-arm MDMs are necessary to provide the coaddition z_{22} and z_{42} modes in non-centered systems (Figure 4-Down). The axial forces $F_{a,k}$ and $F_{c,k}$ for each mode are displayed by Table 2.

6. Degenerated Configurations for Fifth-order Triangle Mode

Degenerated configurations also exist for the *Triangle* 5 mode $z_{33} = A_{33}\ r^3 \cos 3\theta$ with $F_{a,k} = 0$. Such as for *Astm* 3, only $F_{c,k}$ forces can be used for a mirror having an arm-number $k_m \geqslant 6$. These solutions are derived from the condition achieved by Equation (14) and the substitution of the coefficients defined by Equation (11f). The resulting particular geometry is provided by

$$\frac{c}{b} = 1 - \frac{1 + \dfrac{1}{4}(1-\gamma)(1-\nu)\left[2 - \dfrac{5-\nu}{1-\nu}\dfrac{b^2}{a^2} - \dfrac{a^6}{b^6}\right]}{3 + \dfrac{3}{4}(1-\gamma)(1-\nu)\left[2 - \dfrac{7-3\nu}{1-\nu}\dfrac{b^2}{a^2} + \dfrac{a^6}{b^6}\right]}. \tag{27}$$

The geometry of a vase form or a meniscus form satisfying $F_{a,k} = 0$ only use $F_{c,k}$ forces applied at the outer ends of the arms. From the condition (12a), these forces are

$$F_{c,k} = b \int_{\pi(2k-3)/k_m}^{\pi(2k-1)/k_m} V_r(b, \theta) \mathrm{d}\theta. \tag{28}$$

Choosing $k_m = 6$ arm-number, we obtain after integration

$$F_{c,k} = (-1)^k 4(1-\nu)\left(3B_{33} - 6\frac{C_{33}}{b^6} + 2\frac{7-3\nu}{1-\nu} b^2 E_{33}\right) D_2 b \quad \text{with } k = 1, 2, \ldots, 6 \tag{29}$$

and after substitution of the coefficients the six forces are represented by

$$F_{c,k} = (-1)^k 3(1-\gamma)(1-\nu)^2 \left[\frac{4}{(1-\gamma)(1-\nu)} + 2 - \frac{7-3\nu}{1-\nu}\frac{a^2}{b^2} + \frac{a^6}{b^6}\right] D_2 b A_{33}. \tag{30}$$

6.1. Meniscus Form Case

The rigidity-ratio reduces to $\gamma = 1$ and does not depend on the Poisson's ratio in this case. Therefore,

1 → *Three pairs of opposite sets of* $F_{c,k}$ *forces provide Tri 5 if*

$$c/a = c/b = 2/3. \tag{31}$$

2 → *With* $k_m = 6$ *arm menicus, the intensity and the direction of each force is*

$$F_{c,k} = (-1)^k \frac{Et^3 a}{1+\nu} A_{33} \quad \textit{with} \quad k = 1, 2, \ldots, 6. \tag{32}$$

6.2. Vase Form Case

As a general result from formula (27), the c/b ratios for vase forms are larger than those for meniscus forms. This greatly improves the stability of the force equilibrium when loading. For instance, with a $k_m = 6$ arm-number mirror, the $F_{c,k}$ forces are given by Equation (30) and a convenient choice of $(t_2/t_1, b/a)$ in condition (27) allows finding $c = a$ which provides a quite *compact design* (Figure 6).

With vase form mirrors, the extra-thickness $t_2 - t_1$ is laid on only one side: the mirror rear side. So the middle surface is not exactly a sphere (or a plane) of constant curvature but is more curved at its edge towards the rear side. Now, from the point of view

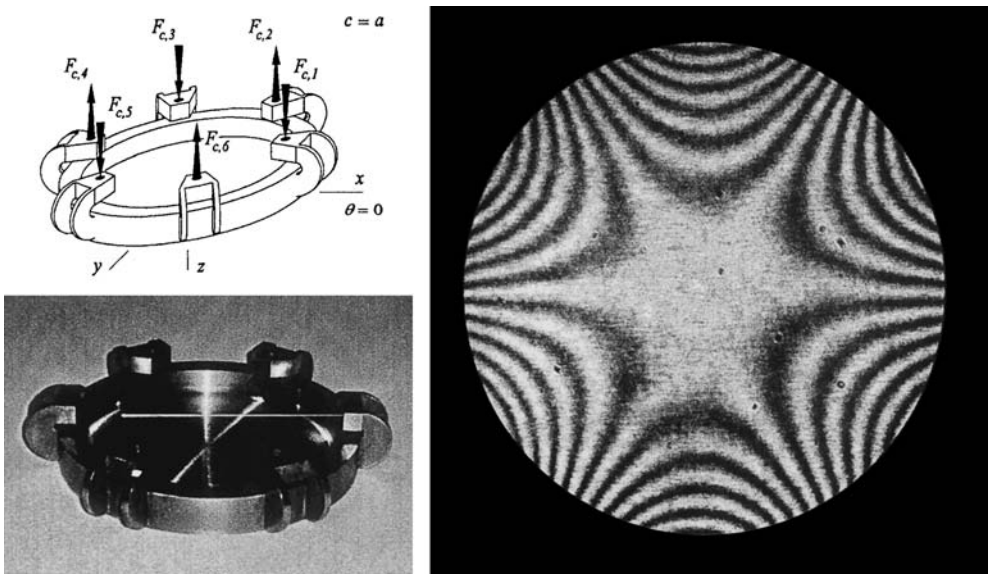

Figure 6. Degenerated configuration of a six-arm *vase form* providing a $Tri5$ mode deflection. This solution satisfies condition (27), expressing that $F_{a,k} = 0$, and then only requires six external forces. Substrate: FeCR13 stainless steel, $\nu = 0.305$. Geometry: clear aperture $2a = 100$ mm, $2a/t_1 = 20$, $t_2/t_1 = 3$, $b/a = 1.2$, $c/b = 0.8382$, then $c/a = 1.0058 \simeq 1$. (*Left*) Design and view of the holosteric mirror. (*Right*) Resulting He–Ne interferogram after deflection. With respect to higher-order modes of the triangle family, the reduction of the interferograms shows that the purity of this mode is characterized by $|A_{53}/A_{33}| \leqslant 0.033$ and $|A_{73}/A_{33}| \leqslant 0.0013$.

of the deformation presently derived from the elasticity theory, the whole middle surface is assumed to be a sphere (or a plane) up to $r = b$. Thus the ring thickness t_2 is theoretically considered as equally distributed on each sides of the middle surface, i.e. in a T-shaped mirror edge. This difference in the shape of the middle surfaces is traduced in practice by a small curvature mode – that may be call $Cv1'$ – that comes in addition to the generated modes. Since MDMs use two forces per arm, the $Cv1'$ effect can be exactly canceled by generating the anti-moments at the contour with those forces. With degenerated configurations, since there is only one force per arm, the exact balance of the azimuthal amplitudes can be recovered either by refocussing or if not possible by polishing the mirror at a new spherical shape changed of the small amount $-Cv1'$. In the present case of generating z_{33} mode, the $Cv1'$ effect is positive i.e. towards z positive. The mirror displayed Figure 6 was designed with a plane surface and polished slightly convex to a clear aperture sag of one He-Ne wavelength for obtaining the balanced interferogram. The $Cv1'$ effect decreases when $t_2 \to t_1$ and becomes zeroed in the case of meniscus mirrors.

7. Conclusion

Vase form MDMs are more efficient than meniscus form MDMs with respect to Saint Venant's principle since with vase mirrors no slope discontinuities that could be due to the shear component of the flexure appear near the location of acting forces. Compared to the zonal retouch method, the *active optics method* with *Clebsch–Zernike modes* shows a large capability to achieve smooth high-order corrections thus providing a significant gain in image quality. This accurate method is of large potential development. Many applications of meniscus form as well as vase form MDMs are: mirrors of future giant telescopes [23], off-axis mirrors for unobstructed large telescopes, aberration corrected mirrors for physics laboratories, aberration corrected diffraction gratings for spectroscopy, and active mirrors for high energy physics.

The development of active optics methods has also led to elasticity investigations on equal curvature cantilever problems [24].

Acknowledgements

The author is grateful to P. Montiel, P. Joulié and P. Lanzoni for the mirror figuring of degenerated configurations (two prototype mirrors have been built for each case presented in Sections 4 and 6), the elaboration of the drawings and figures.

References

1. Lemaître, G.R., 'Active optics and elastic relaxation methods', in: International Commission for Optics 12, *Current Trends in Optics*, Taylor & Francis, London, 1981, 135–149.
2. Lemaître, G.R., 'Various aspects of Active Optics', in: Roddier F.J. (ed.), *Telescopes and Active Systems*, SPIE Proc., **1114** (1989) 328–341.
3. Huber, M.C.E., et al., 'Toroidal grating obtained on elastic substrate: SOHO Mission', *Appl. Opt.* **20** (1981) 2139–2142.
4. Ferrari, M., 'Development of variable curvature mirrors for the delay lines of the VLTI', *A&A Suppl. Ser.* **128** (1998) 221–227.

5. Lubliner, J. and Nelson, J.E., 'KECK Telescope: Stressed mirror polishing', *Appl. Opt.* **19** (1980) 2332–2340.
6. Nelson, J.E., Gabor, J., Lubliner J. and Mast, T., 'KECK Telescope: Stressed mirror polishing', *Appl. Opt.* **19** (1980) 2341–2350.
7. Wang, S-g., Su, D-q., Chu, Y-q., Cui, X-q. and Wang, Y-n., 'Special configuration of a very large Schmidt telescope for extensive astronomical spectroscopic observations - LAMOST', *Appl. Opt.* **35**(25) (1996) 5155–5161.
8. Su, H-j. and Cui, X-q., 'LAMOST Project and its current status', *Large Ground-Based Telescopes*, SPIE Proc. **4837** (2003) 26–35.
9. Wilson, R.N., 'Active optics control systems', *Reflecting Telescope Optics II*, Springer, Berlin, 1999, Chapter 3, 274–314.
10. Schwesinger, G., 'Nondistorting lateral edge support of large telescope mirrors', *Appl. Opt.* **33**(7) (1994) 1198–1202.
11. Noethe, L., 'Active optics in modern large optical telescopes', in: Wolf, E. (ed.), *Progress in Optics*, **43** (2002) 1–69.
12. Timoshenko, S.P., Woinovsky-Krieger, S., *Theory of Plates and Shells*, McGraw-Hill Co., 2nd edition, 1959, p. 284.
13. Borra, E.F., Content, R. and Girard L., 'Optical shop test of f/1.2-2.5 meter diameter liquid mirror', *Ap.J.* **418** (1993) 943–946.
14. Hickson, P., Borra, E.F., Cabanac, R., Chapman, S.C., de Lapparent, V., Mulrooney, M., Walker, G.A., 'Large Zenith Telescope project: A 6-m mercury-mirror telescope', *Advanced Tecchnology Optical/IR Telescopes*, SPIE Proc., **3352** (1998) 226–232.
15. Richardson, E.H., 'Corrector lens design for the UBC 5-m liquid mirror telescope', Report to P. Hickson, University of British Columbia, Vancouver, 1995.
16. Moretto, G., 'Corrector design using vase mirrors for fixed telescope access to large sky areas', *Appl. Opt.* **36** (1997) 10.
17. Moretto, G., Lemaître, G.R., Bactivelane, T., Wang, M., Ferrari, M., Mazzanti, S. and Borra E.F., 'Active mirrors warped using Zernike modes', *A.&A. Suppl. Ser.* **114** (1995) 379–386.
18. Green, J.G., 'The Cosmic Origins Spectrograph : A Hubble replacement instrument', *Space Telescope and Instruments*, SPIE Proc. **3356** (1998) 265–270.
19. Duban, M., 'Third-generation holographic Rowland mounting: third order theory', *Appl. Opt.* **38**(16) (1999) 3443–3449.
20. Duban, M., 'Theory and computation of three COS gratings recorded with MDMS' *Appl. Opt.* **38**(7) (1999) 1096–1102.
21. Lemaitre, G.R. 'New procedure for making Schmidt corrector plates', *Appl. Opt.* **11**(10) (1972) 1630–1636; *Appl. Opt.*, **11**(10) (1972) 2264
22. Lemaitre, G.R. 'Relfective Schmidt anastimat telescopes and pseudo-flat made by elasticiy', *J. Opt. Soc. Am.* **66**(12) (1976) 1334–1340.
23. Dierickx, P., Gilmozzi, R., 'Progress of the OWL 100-m telescope conceptual design', in *Telescope Structures*, SPIE Proc., **4004** (2000) 290–299.
24. Lemaitre, G.R. 'Equal curvature and equal constraint cantilevers', *Meccanica* **32** (1997) 493–503.